

pubs.acs.org/acssensors Article

Catalyst-Free Aqueous Hyperpolarized [1-13C]Pyruvate Obtained by Re-Dissolution Signal Amplification by Reversible Exchange

Andreas B. Schmidt,*,* Henri de Maissin,* Isaiah Adelabu, Shiraz Nantogma, Jessica Ettedgui, Patrick TomHon, Boyd M. Goodson, Thomas Theis, and Eduard Y. Chekmenev*



Cite This: https://doi.org/10.1021/acssensors.2c01715



ACCESS

Metrics & More

Article Recommendations

SABRE-SHEATH

[1-13C]pyruvate
polarization
polarization
polarization
polarization
of hyperpolarized
[1-13C]pyruvate
ethyl acetate

1.4 T

Precipitation with
ethyl acetate

ABSTRACT: Despite great successes in oncology, patient outcomes are often still discouraging, and hence the diagnostic imaging paradigm is increasingly shifting toward functional imaging of the pathology to better understand individual disease biology and to personalize therapies. The dissolution Dynamic Nuclear Polarization (d-DNP) hyperpolarization method has enabled unprecedented real-time MRI sensing of metabolism and tissue pH using hyperpolarized [1- 13 C]pyruvate as a biosensor with great potential for diagnosis and monitoring of cancer patients. However, current d-DNP is expensive and suffers from long hyperpolarization times, posing a substantial translational roadblock. Here, we report the development of Re-Dissolution Signal Amplification By Reversible Exchange (Re-D SABRE), which relies on fast and low-cost hyperpolarization of [1- 13 C]pyruvate by chemical exchange with parahydrogen at microtesla magnetic fields. [1- 13 C]pyruvate is precipitated from catalyst-containing methanol using ethyl acetate and rapidly reconstituted in aqueous media. 13 C polarization of 9 ± 1% is demonstrated after redissolution in water with residual iridium mass fraction of 8.5 ± 1.5 ppm; further improvement is anticipated via process automation. Re-D SABRE makes hyperpolarized [1- 13 C]pyruvate biosensor available at a fraction of the cost (<\$10,000) and production time (≈1 min) of currently used techniques and makes aqueous hyperpolarized [1- 13 C]pyruvate "ready" for in vivo applications.

KEYWORDS: Biosensors, magnetic resonance imaging, hyperpolarization, imaging agents, NMR spectroscopy, Parahydrogen, Pyruvate, SABRE

natomical MRI has become an indispensable tool for Amedical diagnostics, but low sensitivity limits its use to imaging the most abundant substances in vivo: mostly water and lipid protons with few exceptions. The weak detection sensitivity of magnetic resonance (MR) stems from the low degree of nuclear spin alignment (also termed polarization), which linearly increases with the magnetic field of the MRI system. However, even at 7T—the strongest magnetic field used for diagnostics in the US—the nuclear spin polarization (P) of protons is 2.4×10^{-5} or 2.4×10^{-3} %. The MRI signal is directly proportional to P, ultimately meaning that \approx 99.998% of the nuclei are not detected by conventional MRI measurements. For $^{13}\mathrm{C}$, the polarization $(P_{13\mathrm{C}})$ is even lower because of the four times lower gyromagnetic ratio. Nuclear hyperpolarization techniques can provide a transient MR signal enhancement with P of the order of unity. 1,2 This signal gain of 4-6 orders of magnitude has enabled imaging of dilute exogenous biomolecules that are administered as hyperpolarized (HP) biosensors. Imaging of metabolic conversion becomes possible because the administered agent and

metabolic downstream products have different resonance frequencies (chemical shifts).³ Hence, the fate of the metabolites can be mapped *in vivo* over the lifetime of the hyperpolarization (often a few minutes for ¹³C), which is sufficiently long to detect relatively fast metabolic processes like glycolysis and the Warburg effect converting pyruvate to lactate in tumors

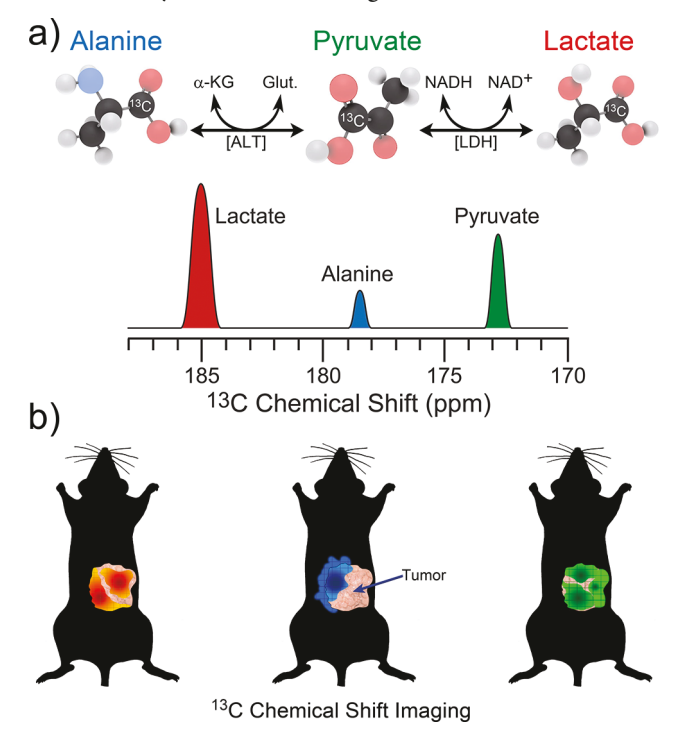
HP [1-¹³C]pyruvate has emerged as the leading HP biosensor due to its central role in cellular energy metabolic pathways and fast cellular uptake.⁴ Specifically, pyruvate is a key downstream metabolite of glycolysis. In cancer and many other diseases, elevated glycolysis leads to anaerobic pyruvate transformation to lactate. As a result, the injection of HP

Received: August 9, 2022 Accepted: October 31, 2022



[1-¹³C]pyruvate leads to its *in vivo* uptake followed by the metabolic transformation to HP [1-¹³C]alanine (via alanine transaminase [ALT]) and to HP [1-¹³C]lactate (via lactate dehydrogenase [LDH]). These three key metabolites can be sensed *in vivo* individually because of the chemical shift

Scheme 1. Magnetic Resonance (MR) Sensing Concept of HP $[1^{-13}C]$ Pyruvate Contrast Agent^a



"(a) Injection of HP [1-¹³C]pyruvate results in its *in vivo* uptake followed by the metabolic transformation to HP [1-¹³C]alanine (via alanine transaminase [ALT]) and to HP [1-¹³C]lactate (via lactate dehydrogenase [LDH]). These three key metabolites can be sensed *in vivo* individually because of the chemical shift dispersion of their HP [1-¹³C] carbon resonances. (b) ¹³C Chemical Shift Imaging (CSI) allows for *in vivo* sensing of each HP metabolite and their individual mapping. Note the color coding of HP [1-¹³C]lactate (red), [1-¹³C]alanine (blue), and [1-¹³C]pyruvate (green). Reproduced with permission from ref 5. Copyright 2015 Wiley.

dispersion of their HP [1-13C] carbon resonances, Scheme 1a. ¹³C Chemical Shift Imaging (CSI) allows for in vivo sensing of each HP metabolite and their individual mapping, Scheme 1b. 5-7 Since the HP [1-13C]pyruvate to HP [1-13C]lactate transformation is upregulated in cancer and other diseases, the metabolic sensing readout of HP [1-13C]pyruvate is useful for monitoring response to treatment and grading of cancer.^{6,8,9} Specifically, the HP [1-13C]lactate to HP [1-13C]pyruvate ratio and LDH activity, which can be sensed by fitting the timeresolved metabolite maps with a kinetic model, represent an effective quantitative sensing method using MRI. MRI technology employs no ionizing radiation. Therefore, MRI with the HP [1-13C]pyruvate contrast agent offers substantial sensing advantages compared to Positron Emission Tomography (PET), which employs the radioactive ¹⁸F-fluorodeoxyglucose tracer to probe elevated glucose uptake. 10 The MRI scan using HP [1-13C]pyruvate contrast agent can be completed in approximately 1 min (from injection to the

end of sensing), and same-day follow-up scans can be performed in principle, since no background signal from injected HP [1- 13 C]pyruvate remains after 10 min. In contrast, FDG-PET scans takes approximately 1.5–2 h (from injection to the end of sensing), and the follow-up scan is typically performed ≥ 6 weeks after the initial scan to minimize patient radiation exposure. Moreover, FDG-PET scans enable sensing of FDG uptake, but metabolic conversion is not detected, whereas the use of the HP [1- 13 C]pyruvate contrast agent allows direct sensing of real-time metabolism.

The HP [1-¹³C]pyruvate contrast agent is now under evaluation in over 30 clinical trials according to clinical-trials.gov. These promising clinical sensing studies employ the dissolution Dynamic Nuclear Polarization (d-DNP) hyperpolarization technique for production of HP [1-¹³C]-pyruvate. Despite the success of d-DNP, this method still suffers from high instrumentation cost (>\$2M) and complexity, as well as low agent throughput (approximately one polarized batch per hour using the most recent instrumentation). Impressive methodological and technical advances are being made for the technique; 11-13 however, more efficient and cost-effective approaches are desirable to make HP [1-¹³C]pyruvate readily accessible to the biomedical community with the ultimate goal of translation to routine clinical use.

Two fast hyperpolarization approaches have been introduced for [1-13C]pyruvate using the spin order provided by parahydrogen (p-H₂)—the nuclear spin singlet state isomer of H₂ gas. 14-16 Reineri et al. have employed the Parahydrogen Induced Polarization (PHIP) method 17,18 to hydrogenate an unsaturated side arm of esterified [1-13C]pyruvate; 19 this side arm hydrogenation (SAH) PHIP method has now been utilized and adapted by several groups. 20-23 Cleavage of the side arm and extraction into aqueous media was demonstrated in a few studies. 24-28 Duckett et al. pioneered the nonhydrogenative Signal Amplification by Reversible Exchange (SABRE) approach.²⁹ This method is based on the simultaneous, temporary binding of a substrate and p-H2 to an Ir-hexacoordinate complex. This transient complex enables polarization transfer from p-H2-derived hydrides to the substrate via scalar couplings. SABRE in SHield Enables Alignment Transfer to Heteronuclei (SABRE-SHEATH) is a SABRE variant that achieves efficient direct hyperpolarization of heteronuclei by performing the exchange reaction at sufficiently low magnetic field (typically hundreds of nanotesla).³⁰ At these fields, polarization can be spontaneously transferred from p-H2-derived hydrides to the 1-13 C nucleus of pyruvate. When the transient complex dissociates, free HP [1-13C]pyruvate can be generated in solution in less than 1 min. P_{13C} of order unity has been demonstrated on the catalyst-bound [1- 13 C]pyruvate and $P_{13C} \approx 13\%$ in the "free" state at relatively high (30 mM) pyruvate concentration.^{31–33} Rapid increase of the temperature (referred to as temperature cycling) has been shown to effectively release the pyruvate from the catalyst to obtain highly polarized solutions of [1-13C]pyruvate in CD₃OD.³⁴

Despite these relatively large pyruvate $P_{\rm 13C}$ values achieved by SABRE, the approach has been limited to preparing pyruvate solutions in methanol in the presence of a few-millimolar iridium-based catalyst. This HP formulation is not suitable for direct biomedical use. A number of previous purification approaches have been demonstrated to capture Ir-IMes catalyst, $^{35-37}$ but have not been applied to produce HP

[1-¹³C]pyruvate. Moreover, pyruvate reconstitution from toxic methanol remains an unaddressed challenge.

Here, we address these shortcomings of SABRE hyperpolarization and introduce Re-Dissolution (Re-D) SABRE for the production of an aqueous, catalyst-free (residual Ir mass fraction of 8.5 \pm 1.5 ppm) 6 mM HP [1- 13 C]pyruvate formulation with $P_{13\rm C}\approx9\pm1\%$. First, the microtesla relaxation and polarization build-up dynamics reveal that nondeuterated methanol can be employed as efficiently as CD₃OD for [1- 13 C]pyruvate hyperpolarization. Second, precipitation of HP [1- 13 C]pyruvate from the organic solvent followed by a rapid dissolution of the microcrystalline phase into aqueous media preserves the polarization and an aqueous HP solution is obtained. We perform systematic 13 C relaxation studies indicating that the lifetime of HP [1- 13 C]pyruvate is strongly modulated during the phase transitions.

■ EXPERIMENTAL SECTION

Parahydrogen was enriched to >99.10% (as confirmed by benchtop NMR spectroscopy) and filled into aluminum cylinders at 350 psi using a setup described previously.³⁸ The SABRE samples were prepared in CD₃OD, CH₃OH, or ethanol using the stated concentration of sodium [1-¹³C]pyruvate, 6 mM iridium catalyst, and 40 mM dimethyl sulfoxide (DMSO) as described previously.^{31,34} For the SABRE experiments, the samples were filled into 5 mm NMR tubes. For precipitation of pyruvate, room temperature ethyl acetate (EtAc) was added to the samples. In the case of redissolution SABRE (Re-D SABRE), room-temperature H₂O or D₂O was added to reconstitute the pyruvate in water.

For SABRE-SHEATH hyperpolarization, we employed a previously reported setup and experimental protocol, Figure 1a. 31,34 In brief, the setup consisted of a 3-layer mu-metal of 3" I.D. and 9" depth to shield external magnetic fields, combined with a custom-made solenoid to generate a static magnetic field B_0 of $\approx 0.4~\mu T$. The sample NMR tubes were mounted to a gas-flow setup to guide pressurized (100 psi, i.e., ≈ 8 bar total pressure) p-H₂ through the solution at a flow of 75 scc/m to activate the catalyst and to 13 C-hyperpolarize sodium [1- 13 C]pyruvate solutions. Activation of the catalyst took place for 2 min at ambient temperature and magnetic field. For polarization build-up, the sample was placed in the static magnetic field (typically $\approx 0.4~\mu T$) and a water bath to regulate the reaction temperature.

For precipitation and redissolution of HP [1-13C]pyruvate, a phase separation approach was applied, Figure 1b, exploiting that water and EtAc are immiscible. The precipitation was performed in the same NMR tube where hyperpolarization took place. 400 μ L EtAc was added quickly to the sample consisting of 100 μ L of 30 mM HP [1- 13 C]pyruvate, right after removing this sample from the 0.4 μ T field and releasing the pressure ($\approx 3-4$ s). To mix the solution after EtAc addition, further p-H2 bubbling was used at a low flow rate (\sim 5–10 scc/m, ambient pressure). For redissolution, 300 μ L water were added directly to the NMR tube with the precipitate-containing solution, and again, gas flow was used to mix and dissolve the pyruvate microcrystals. After mixing the solutions, most of the aqueous phase rapidly separated from the organic phase (≈ 1 s). Typical precipitation time was $t_{\rm prec} \approx 2$ s and water addition time $t_{\rm water}$ \approx 6 s, where t_{water} consisted of 1 s to add water, plus 4 s to bubble gas, and 1 s to settle the solution (see Figure S9 for more information). We found that adding EtAc in this ratio of 4 to 1 to the HP sample precipitated most of the pyruvate (62 ± 11%, Figure S9) and after redissolution, 39 ± 1% of the HP pyruvate was transferred to the aqueous phase (Table S3). Using this protocol, the obtained twophase samples visibly contained a major fraction of the catalyst in the organic phase (which remained yellowish and turned reddish after exposure to atmosphere, Figure S7), whereas a clear aqueous solution of total volume of $\approx 335 \pm 10 \ \mu L$ was obtained (as detailed below approximately half of the CH₃OH remained in the aqueous phase), Figure S6. The total volumes of the investigated mixtures containing the precipitate were approximately 500 μ L (3.9 cm fill height in the

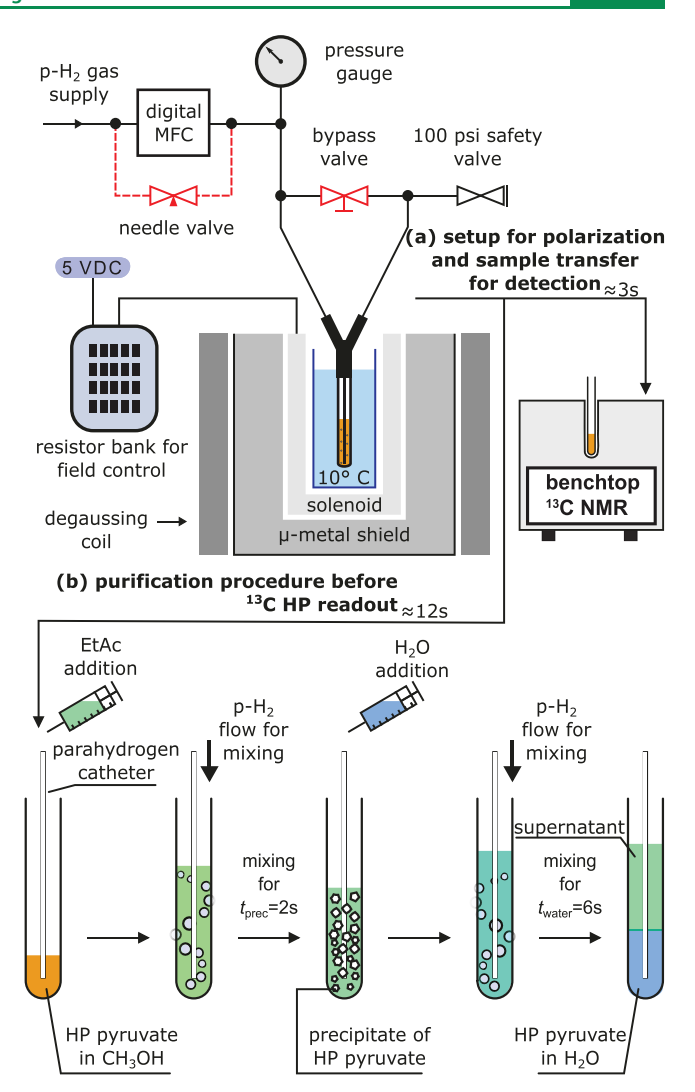


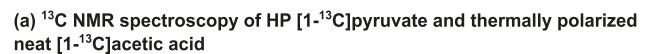
Figure 1. (a) Schematic of SABRE-SHEATH setup. Pressurized p-H₂ (8 bar total pressure using 100 psi overpressure regulated by a safety valve) was guided through the sample held in a 5 mm NMR tube at a flow rate of 75 scc/m using a digital mass flow controller (MFC). For the mixing step in the Re-D SABRE-SHEATH experiments, the same bubbling setup was used but the MFC was turned off and bypassed using a needle valve adjusting the flow to $\approx 5-10$ scc/m (due to MFC instability at low scc/m rate). For hyperpolarization, the sample containing pyruvate and catalyst in CH₃OH was placed in a coldwater bath held inside a mu-metal shielded electromagnet adjusting the magnetic field to $\approx 0.4 \mu T$. HP 13 C signals were detected after transferring the samples into a benchtop 1.4T NMR system next to the SABRE-SHEATH setup. (b) Schematic of additional purification procedure steps employed for Re-D SABRE after the sample removal from the shield and before the ¹³C NMR signal detection: HP [1-13C]pyruvate was precipitated from the organic phase by adding ethyl acetate (EtAc), redissolved in water, followed by the phase separation.

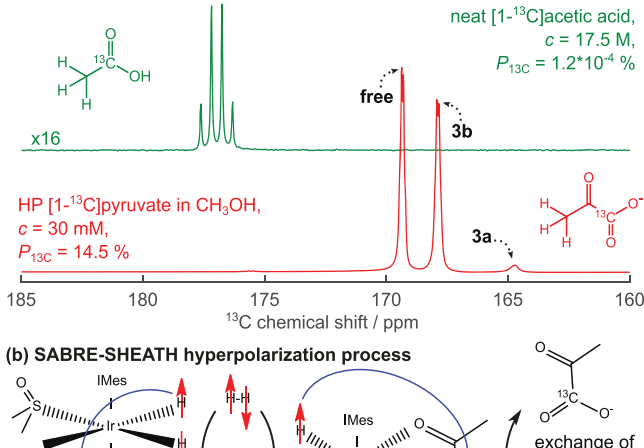
NMR tube), and after the addition of water the total fluid volume was $\approx 800~\mu L$ (≈ 6 cm fill height). During the phase mixing, parts of the sample were lifted by approximately 5 cm by the ascending p-H₂ gas bubbles. The sample height in the NMR tube was the decisive factor affecting our choice of solvent volumes to minimize the mixtures from leaving the 1.4T field of the benchtop NMR spectrometer (approximately 10 cm along the sample tube) as much as possible. At the same time, 300 μL water were added despite significantly diluting the smaller initially polarized 100 μL of 30 mM [1-¹³C]-pyruvate batch to fill the sensitive NMR detection volume in the

spectrometer to avoid detrimental line broadening that could otherwise affect the quantification. These limitations are clear shortcomings of our current experimental design and can be remedied in the future with purpose-built hyperpolarization equipment. Additional experimental details are presented in the SI.

RESULTS AND DISCUSSION

SABRE-SHEATH Polarization of [1-¹³**C]Pyruvate.** High $P_{13\text{C}}$ of up to \approx 14.5%, i.e., a ¹³C signal enhancement $\varepsilon_{13\text{C}}$ of \approx 100,000-fold, of 30 mM [1-¹³C]pyruvate was achieved in methanol, which was confirmed after transferring the HP samples from the polarizer into a 1.4T benchtop ¹H/¹³C NMR system. The mean of N=19 experiments from 9 samples measured on 5 different days under the same conditions was 8 \pm 2%. Figure 2a shows the spectrum of HP [1-¹³C]pyruvate





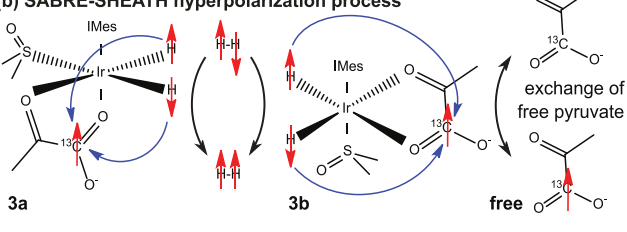


Figure 2. SABRE-SHEATH hyperpolarization of $[1^{-13}C]$ pyruvate: (a) ^{13}C NMR spectroscopy of HP $[1^{-13}C]$ pyruvate; note the three HP resonances corresponding to the species described in display b. (b) Schematic of simultaneous p-H $_2$ and $[1^{-13}C]$ pyruvate binding to the Ir-based catalyst in two different forms as described by Duckett et al.: 32 3a and 3b; note pyruvate binding to 3a is irreversible on the experimental time scale; thus, only 3b is SABRE-active resulting in build-up of free HP $[1^{-13}C]$ pyruvate over time in a submicrotesla magnetic field, Figure 3a below. [IrCl(COD)(IMes)] precatalyst was used (IMes = 1,3-bis(2,4,6-trimethylphenyl)imidazol-2-ylidene; COD = cyclooctadiene)]).

versus the signal from a corresponding reference spectrum of thermally polarized [1- 13 C]acetic acid (17.5 M, $P_{13C} \approx 1.2 \times 10^{-6}$ at $B_0 = 1.4$ T). Optimal experimental parameters were used as identified in Figure 3.

[1-¹³C]Pyruvate Polarization Dynamics in Protonated Methanol and Ethanol Solvents. CD₃OD is widely used as the SABRE-reaction-hosting solvent because it provides a convenient means of attaining high-field NMR spectrometer lock. However, nondeuterated polarization media may be preferred for biomedical applications. For this reason, we performed systematic dynamics studies comparing CD₃OD, CH₃OH, and C₂H₃OH for SABRE-SHEATH [1-¹³C]pyruvate hyperpolarization for fixed concentrations of pyruvate, SABRE catalyst, and DMSO (30 mM, 6 mM, and 40 mM,

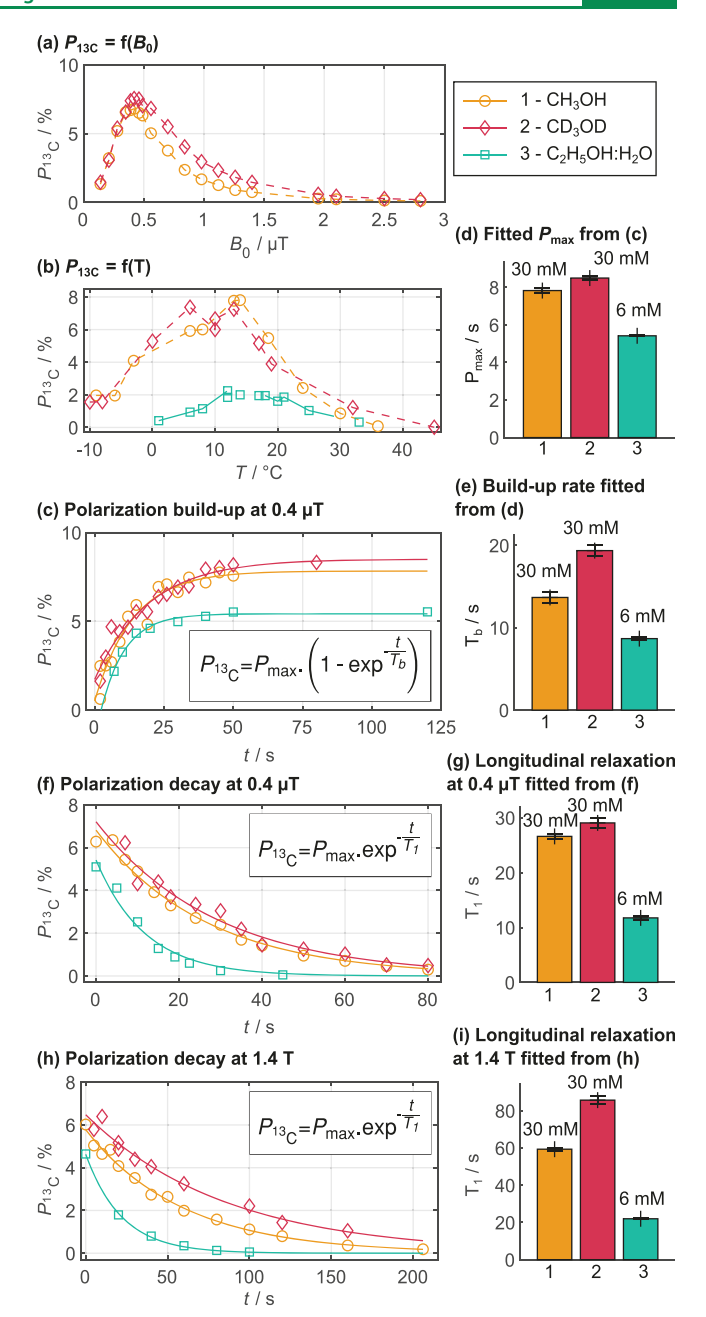


Figure 3. SABRE polarization dynamics. The dynamics were analyzed in three different solvents, namely, CH₃OH (orange, circles), CD₃OD (red, diamonds), and a mixture of 90% C₂H₅OH and 10% H₂O (green, squares) using concentrations of [1-13C]pyruvate, SABRE catalyst, and DMSO of 30 mM (6 mM for C₂H₅OH+10% H₂O), 6 mM, and 40 mM, respectively. The SABRE-SHEATH hyperpolarization of [1-13C]pyruvate was investigated as a function of the magnetic field B_0 (a), reaction temperature T (b), time for polarization build-up at 0.4 μT (c) with corresponding extracted values of P_{max} (d), and build-up rate (e), T_1 relaxation of the ^{13}C hyperpolarization monitored at 0.4 μT (f) and corresponding bar chart of extracted T_1 values (g), and T_1 relaxation of the 13 C hyperpolarization monitored at 1.4 T (h) and corresponding bar chart of extracted T_1 values (i). The substantially reduced 13 C T_1 of ethanol samples are likely due to a higher catalyst:substrate ratio (1:1 vs 1:5 for methanol samples). See SI for more details.

respectively). However, the ethanol sample was prepared with only 6 mM pyruvate and 10% H_2O due to limited solubility. The optimal B_T was similar in all investigated

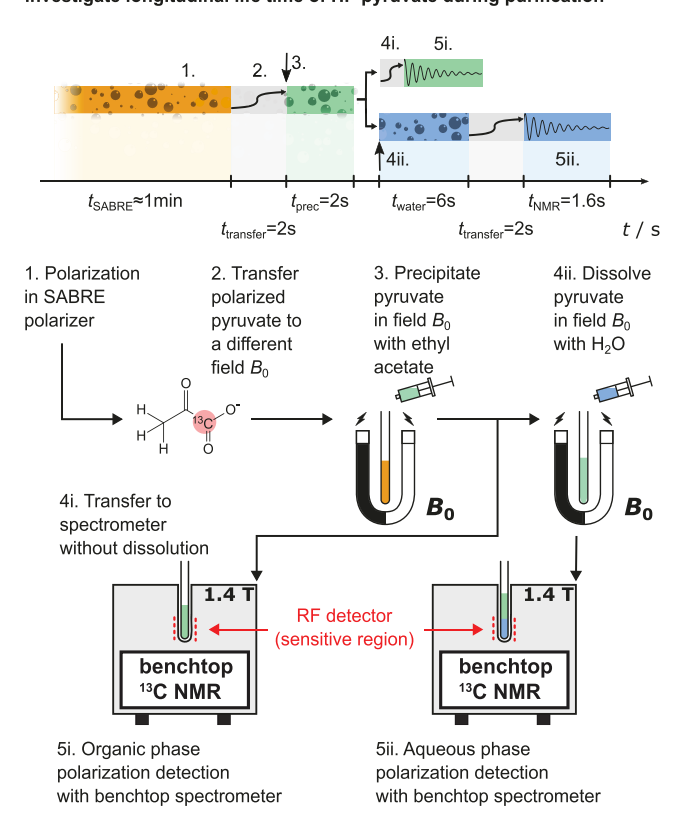
samples (\approx 0.4 μ T, Figure 3a). The highest [1-¹³C]pyruvate polarizations were observed at $T_{\rm T}$ = 9–14 °C in both methanol samples and for ethanol at 12–18 °C (Figure 3b). Thus, all the experiments described below were performed using these optimized $B_{\rm T}$ and $T_{\rm T}$ parameters.

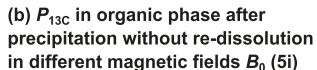
We found that the hyperpolarization was similarly effective in CD₃OD and CH₃OH. The polarization build-up (T_b) and decay (T_1) at 0.4 μ T were similar: $T_b = 13.7 \pm 0.6$ s versus 19.3 \pm 0.6 s; and T_1 = 26.0 \pm 0.4 s versus 29.1 \pm 0.8 s, respectively (Figure 3c,e). P_{13C} values were also similar; in one representative example of polarization build-up, P_{13C} was 7.8 \pm 0.1% vs 8.5 \pm 0.1% for CH₃OH and CD₃OD media, respectively, Figure 3d. The ¹³C T₁ relaxation time at high field (i.e., a clinically relevant field of 1.4T) was significantly greater in the deuterated solvent, 86 ± 2 s versus 59.3 ± 0.8 s. For ethanol, 1.4-fold lower P_{13C} values were obtained in this mixture compared to CH₃OH and CD₃OD, which is rationalized by a more efficient relaxation at the SABRE-SHEATH field, Figure 3e. Hence, despite the higher biocompatibility of ethanol, CH₃OH was selected as the solvent for further experiments due to higher sodium pyruvate solubility, longer relaxation times, and higher P_{13C} levels.

Precipitation of Pyruvate from Solutions. Although previous studies have demonstrated the direct SABRE polarization in biocompatible solvents such as aqueous media, the resulting polarization is markedly (by an order of magnitude or more) reduced compared to that in methanol, presumably due to lower hydrogen solubility and other compounding factors.^{39–45} As a result, we continued with methanol as solvent for SABRE-SHEATH, and investigated the idea of performing precipitation and purification of the HP biomolecule, inspired by Eills, Knecht, and co-workers who used a related approach for fumarate. 46,47 In those studies the precipitation was achieved by adding an acid to the 13Chyperpolarized solutions, whereas here precipitation of pyruvate is achieved by addition of a nonpolar solvent. The present strategy may be advantageous for future clinical applications, because it avoids the use of strong acids and bases immediately before in vivo administration, which leads to additional purification and quality-assurance steps, posing translational challenges. We performed systematic screening of the solvent used for precipitation to meet the following requirements: (a) low solubility of sodium pyruvate to initiate the precipitation; (b) high solubility of the SABRE catalyst to enable its removal from the HP sample; (c) miscibility with methanol to achieve rapid mixing of solutions and pyruvate precipitation; and (d) low toxicity. The screening (see SI for details) revealed that among the options tested, EtAc provided the best performance.

Re-Dissolution (Re-D) SABRE at Different Magnetic Fields. Re-D SABRE was performed at (i) Earth's field, (ii) 10 mT, (iii) 0.3T, and (iv) 1.4T, and the samples were then rapidly transferred to the benchtop 1.4T NMR for detection and quantification of hyperpolarization, such that the aqueous phase was approximately centered in the radiofrequency coil, Figure 4a. In case (iv), for which no transfer was needed, a \approx 5 s delay was added to the end of the protocol for consistency with the time needed to transfer the samples in (i–iii). We expected that low field substantially reduces the hyperpolarization lifetimes in the precipitate; hence, precautions were taken to prevent samples from leaving the studied magnetic fields (i–iv). More details on the experiment setups are reported in the SI.

(a) Experimental procedure for precipitation and re-dissolution to investigate longitudinal life time of HP pyruvate during purification





(c) P_{13C} in aqueous phase after precipitation and re-dissolution in different magnetic fields B₀ (5ii)

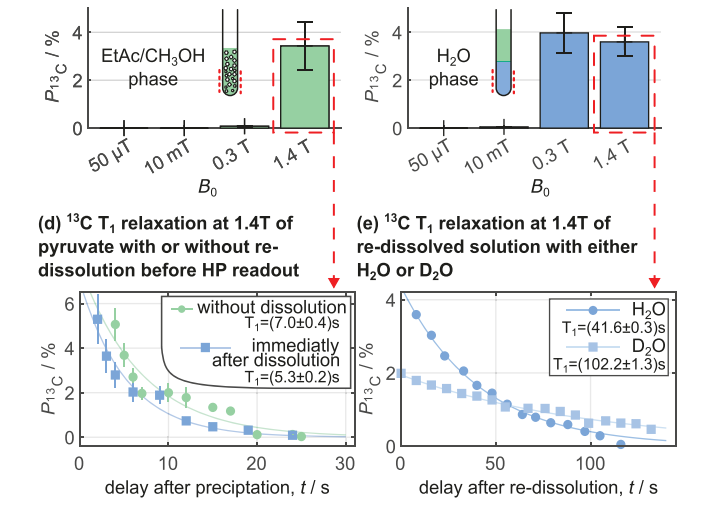


Figure 4. (a) Schematic of the procedure for HP $[1^{-13}C]$ pyruvate precipitation and Re-D SABRE at different magnetic fields. All data was acquired at 1.4 T approximately starting 10 s (b,d) or 16 s (c,e) after hyperpolarization, and either the precipitated samples were moved into the 1.4 T magnet and detected directly (to detect pyruvate dissolved in the supernatant, b and d) or water was added, and samples were agitated at the respective precipitation field before moving the sample to the detection 1.4 T field (c,e). In (d), the data represented by squares was measured after transfer and redissolution at 1.4T. See SI for more details. (b) Dependence of P_{13C} on the magnetic field value employed during HP $[1^{-13}C]$ pyruvate precipitation—note the precipitate was not dissolved, and ^{13}C signal is measured from residual dissolved $[1^{-13}C]$ pyruvate in organic solvent. (c) Dependence of P_{13C} on the magnetic field value employed during

Figure 4. continued

HP $[1^{-13}C]$ pyruvate precipitation and redissolution—note the precipitate was dissolved, and ^{13}C signal is now measured from both the residual dissolved $[1^{-13}C]$ pyruvate that remained dissolved in organic solvent and from the redissolved precipitate. (d) Lightgreen trace: T_1 decay of ^{13}C HP signal measured from the residual dissolved $[1^{-13}C]$ pyruvate in organic solvent (without precipitate dissolution), and dark-green trace: T_1 decay of ^{13}C HP signal measured from both the residual dissolved $[1^{-13}C]$ pyruvate in organic solvent and redissolved HP $[1^{-13}C]$ pyruvate precipitate (data was obtained from the aqueous phase with precipitate dissolution). All data in (d) were obtained from single point acquisitions and separate runs. (e) ^{13}C T_1 decay of HP $[1^{-13}C]$ pyruvate after redissolution SABRE procedure in aqueous media (H_2O) and D_2O respectively used for the redissolution procedure).

No HP 13C signal was observed for the samples with dissolution at Earth's field (i), whereas the 10 mT magnet (ii) still provided P_{13C} = 0.05 \pm 0.02%. In sharp contrast, performing redissolution SABRE at the higher fields, (iii) and (iv), provided much higher $P_{13C} = 4.0 \pm 0.8\%$ (N = 2) and $P_{13C} = 3.6 \pm 0.6\%$ (N = 3), respectively, Figure 4c (3.5 ± 0.4) mM HP [1- 13 C] pyruvate in the $\approx 335 \mu$ L aqueous sample, i.e., $39 \pm 1\%$ of the starting quantity, Table S3). We conclude that precipitated sample exposure to fields below 0.3T may be detrimental to P_{13C} —in line with the observation of no detectable P_{13C} using a precipitate filtering approach performed at 10 mT fields, see SI. It should be noted that no additional data points were taken between 10 mT and 0.3 T—therefore, the lower magnetic field limit at which Re-D SABRE could be performed successfully could be substantially lower than 0.3 T. More systematic relaxation dynamics studies are certainly warranted in the future.

The aqueous solution of HP [1^{-13} C]pyruvate contained residual CH₃OH (2.4 ± 0.3 M, i.e., reduced by an order of magnitude, \approx 2-fold as half the CH₃OH remained in the supernatant and additional 3.35-fold due to dilution) and EtAc (0.8 ± 0.2 M), Table S3 (N = 10 samples). Elemental analysis revealed 8.5 ± 0.5 ppm mass fraction of Ir metal present in the aqueous phase (Table S4), corresponding to a reduction of Ir concentration by \approx 135 fold (by 40-fold due to catalyst partitioning and additional 3.35-fold due to dilution), Figure S7.

Lifetime of Polarization in the Precipitated and Aqueous Samples. To investigate the impact of precipitate relaxation in variable magnetic fields during the redissolution process, the Re-D SABRE experiment was repeated, omitting the addition of water after precipitation (i.e., the decay of ¹³C HP signal in the dissolved phase of the precipitated samples was measured). In both settings with low field (i and ii) no measurable ¹³C polarization was observed, Figure 4b. For (iii), P_{13C} was still much lower compared to the sample that rested at the 1.4T magnet (setup (iv), i.e., P_{13C} = 0.08 \pm 0.02% and P_{13C} = 3.4 ± 0.9%, respectively—this signal is entirely derived from the remaining dissolved pyruvate in solution (2.3 \pm 0.6 mM in the 500 μ L sample of EtAc and CH₃OH, Figure S9) not from the precipitated microcrystalline phase. P_{13C} comparison in setup (iii) and (iv) in Figure 4b suggests that the dissolved-phase HP [1-13C]pyruvate in the EtAc fraction is extremely sensitive to low field exposure: P_{13C} in (iii) was ≈ 40 times lower than P_{13C} in (iv). However, in Figure 4c, we observe that P_{13C} losses are similar when the entire process is contained at 0.3T (iii) and 1.4T (iv) revealing that HP

 $[1^{-13}C]$ pyruvate in the aqueous phase is relatively immune to low-field exposure, and microcrystal exposure to fields as low as 0.3T is not detrimental to P_{13C} . This observation is important because it means the Re-D SABRE process can be successfully performed at storage fields as low as 0.3T. The rapid ^{13}C T_1 of HP $[1^{-13}C]$ pyruvate in the EtAc fraction at Earth's field, estimated to be <1.3 s, may be caused by the high catalyst:substrate ratio in the EtAc.

Finding the surprisingly short T_1 in Earth's field, the T_1 of the precipitated sample phases was measured at 1.4T in configuration (iv). HP signals were measured as a function of an additional delay t_d (ranging from 0 to 23 s; $t = t_{prec} + t_d$), during which P_{13C} was allowed to decay. At the end of $t_{\rm d}$, the signal was detected either immediately (green circles, Figure 4d, sampling the decay rate of the residual dissolved-phase pyruvate) or after the redissolution in D2O (blue squares, Figure 4d, sampling the decay rate of the entire pyruvate (precipitated and dissolved) pool). Assuming a monoexponential decay, the apparent 13 C T_1 was 7.0 ± 0.4 s or 5.3 ± 0.2 s, respectively. These T_1 times are surprisingly short and deserve future detailed investigations. In sharp contrast, T_1 values in the aqueous phase measured after the Re-D SABRE process were 41.6 ± 0.3 s in H₂O and 102 ± 1.3 s in D₂O, Figure 4e, using a series of pulse-detect NMR experiments with low flip angle of 9° (N = 2).

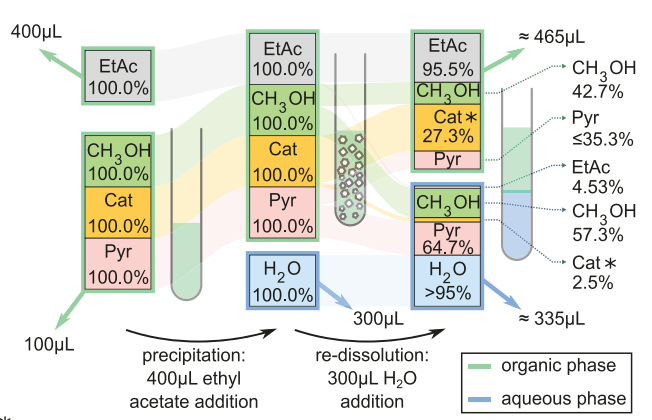
Naturally, a longer T_1 in the precipitated phase would be helpful to retain a higher fraction of produced hyperpolarization. Hence, future investigations should consider evaluation of T_1 at different temperatures, magnetic fields, residual O_2 content, and precipitating solvent composition, or as a function of pH. Although high Re-D SABRE polarizations were obtained above (Figure 2), on average only $\approx 39\%$ of the initial [1-13C]pyruvate was transferred into the aqueous phase in that protocol (determined by high-resolution NMR, Table S3). This observation may be attributable to an inefficient mixing of phases.

Maximizing P_{13C} and Extraction of Aqueous [1-¹³C]-Pyruvate and Trace Analysis of the Obtained Solutions. A more rigorous phase mixing protocol was tested, where the bubbling tube was moved up and down rapidly three times for phase mixing during the $t_{\rm water} \approx 6$ s mixing time. Using this procedure (N=2), $65\pm7\%$ of the initial pyruvate were extracted (vs $\approx 39\%$ as described above) into the aqueous phase, as confirmed by high-resolution NMR spectroscopy, Figure S8. Considering the final volume of the aqueous phase of $335\pm10~\mu{\rm L}$ and the measured pyruvate concentration of 5.8 ± 0.8 mM (in the diluted Re-D SABRE sample), the detected $^{13}{\rm C}$ signals corresponded to a nuclear polarization of $P_{13{\rm C}}=9\pm1\%$ or $8\pm1\%$, i.e., $\varepsilon_{13{\rm C}}$ of $\approx 75,000$ at $1.4{\rm T}$, respectively, N=2 samples, Figure 5.

The reproducibility of our SABRE-SHEATH polarization experiment should be noted, which exhibits large statistical deviations (maximum of P_{13C} = 14.5%, but 8 \pm 2% was the interday mean with standard deviation). Future setup automation of the hyperpolarization and sample shuttling procedure and more standardized experimental and sample preparation protocols are anticipated to improve the reproducibility and mean P_{13C} values before and after HP $[1^{-13}C]$ pyruvate sample purification.

We introduced and demonstrated Re-D SABRE for the production of an aqueous, catalyst-free solution of HP [1- 13 C]pyruvate with $P_{13C} \approx 9 \pm 1\%$. To this end, the microtesla relaxation and polarization build-up dynamics

(a) Sankey diagram of the re-dissolution SABRE purification procedure



*catalyst quantification with elemental analysis did not account for 100% of the starting amount likely due to:
-catalyst loss due to deposition on the walls of NMR tube
-relatively long delay (of a few days) between sample collection and elemental analysis measurements.

(b) ¹³C NMR spectroscopy of HP [1-¹³C]pyruvate and thermally polarized external signal reference neat [1-¹³C]acetic acid

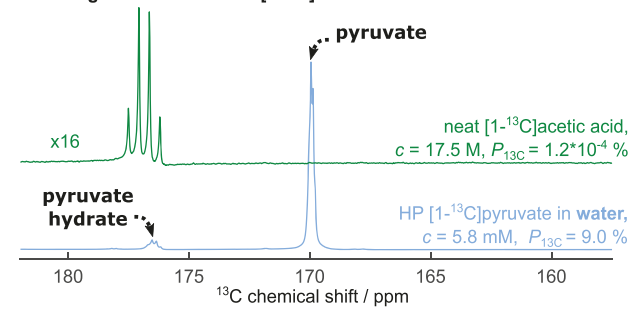


Figure 5. Maximum P_{13C} levels and sample analysis of HP $[1^{-13}C]$ pyruvate in the precipitated and Re-D SABRE samples. (a) Sankey diagram of the procedure showing fractions of the used substances and solvents during the purification process in in the final phase-separated samples for the example experiment shown in (b). (b) ^{13}C signals of a thermally polarized reference (neat $[1^{-13}C]$ acetic acid, $P_{13C} \approx 0.00012\%$, $c \approx 17.5$ M ^{13}C) and HP $[1^{-13}C]$ pyruvate extracted into H_2O , $P_{13C} = 9 \pm 1\%$, $c = 5.8 \pm 0.8$ mM (Figure S8), respectively. Note that the pyruvate sample was diluted by a factor of ≈ 3.35 compared to the initial HP sample of 30 mM pyruvate in methanol to fill the sensitive detection volume of the benchtop NMR, i.e., $65 \pm 7\%$ of the original HP pyruvate was transferred into the H_2O (Figure S8).

revealed that nondeuterated methanol can be employed as efficiently as CD_3OD for $[1^{-13}C]$ pyruvate hyperpolarization. Precipitation of HP $[1^{-13}C]$ pyruvate from the organic solvent followed by a rapid dissolution of the microcrystalline phase into aqueous media preserved the polarization, and an aqueous HP solution was obtained.

We performed systematic 13 C relaxation studies indicating that the lifetime of HP $[1^{-13}\text{C}]$ pyruvate is strongly modulated during the phase transitions: We found that precipitated sample exposure to fields below 0.3T is detrimental to $P_{13\text{C}}$ —in line with the observation of no detectable $P_{13\text{C}}$ using a precipitate filtering approach performed at 10 mT fields; see SI. In addition, after precipitation relatively fast relaxation was observed.

Based on the presented pilot studies, we envision several possible improvements to yield more concentrated and polarized HP $[1-^{13}C]$ pyruvate with lower concentration of the residual solvent for the future Re-D SABRE implementations:

First, SABRE-SHEATH hyperpolarization can also be effective at higher $[1-^{13}C]$ pyruvate concentration in the initial CH₃OH solution, e.g., at 60 mM as demonstrated recently.³⁴

Second, a larger hosting magnet can enable the use of a larger purpose-built reactor to potentially allow improving the ratio of the initial volume of polarized [1^{-13} C]pyruvate solution to the final aqueous HP sample volume to yield higher HP [1^{-13} C]pyruvate concentration in the final aqueous solution. In addition, a larger reactor may allow adding more EtAc to achieve a greater EtAc:CH₃OH ratio for more efficient pyruvate precipitation from the supernatant, and also to absorb more CH₃OH to reduce its concentration in the final aqueous solution; see Table S1.

Third, rapid filtering of the precipitate appears to be a promising alternative to the phase separation method employed here. Indeed, we performed initial tests with commercial 0.2 μ m syringe filters and cotton-filled syringe-based filtration columns clearly showing that most (>99%) of the organic solvent and catalyst can be effectively removed and the precipitate pyruvate can be recovered in neat water after redissolution from the filter, SI section 6. However, the manual implementation of these two filtration alternatives consumed 1–2 min when performed manually, and therefore, we did not observe HP 13 C signals with these approaches, consistent with the results presented above.

Fourth, the relatively short 13 C T_1 in the precipitate implies that future efficient precipitation and redissolution procedures would need to be performed quickly on the time scale of a few seconds. Thus, rapid automated purification of the samples can potentially minimize T_1 -associated polarization losses and therefore yield a better polarized product with less contamination. Note that rapid purifications have been already established in the literature for hydrogenative PHIP techniques and allowed production of solutions, in which traces of solvents, catalyst, and side products of the hydrogenation were below recommended limits for patient applications. ^{26,47,48} Hence, these other promising advances bode well for producing biocompatible HP [1- 13 C]pyruvate via the presented Re-D SABRE approach for widespread, cost- and time-efficient preclinical and clinical future applications.

Translational Outlook. The work reported here has demonstrated that highly polarized aqueous [1-13C]pyruvate solutions can be generated in less than 2 min. The key advantages of this approach are its simplicity and the low cost $(\approx $20,000)$ of the instrumentation, requiring no cryogenic equipment. Only sodium [1-13C]pyruvate, parahydrogen, and SABRE catalyst are required as key reagents. While the cost of the [1-13C]pyruvic acid employed in d-DNP is similar to the cost of sodium [1-13C]pyruvate, it should be noted that d-DNP technology employs expensive instrumentation (\$2M) and offers a substantially slower hyperpolarization production time of ca. 1 h. In the context of ultimate clinical use, a requirement of a multimillion-dollar investment by a clinical practice represents a substantial commitment and does embody an obstacle to widespread use. Indeed, the total cost of producing each batch of HP [1-13C]pyruvate in a patient-ready formulation is a key determinant in facilitating the translation of the approach toward ultimate clinical practice, and that cost includes not only the cost of raw materials but also all of the added costs associated with the purchasing, siting, maintenance, and operation of any involved instrumentation.

Limitations of This Study and Future Directions. As described above, this study revealed unusually fast relaxation

dynamics of HP [1-13C] pyruvate in the precipitated state. This efficient relaxation of the HP state clearly represents a limitation of the approach, which can be potentially solved in the future through process automation to substantially reduce the amount of time needed for the required procedures to ensure that hyperpolarization losses due to sample manipulation will be relatively small. Moreover, this study was substantially constrained by the size of the available magnets, which has limited the sample size to 0.1 mL of the starting HP solution. Because of the small volume of the starting solution and the requirements to have at least 0.3 mL of the final aqueous-media solution, the experiments resulted in the overall dilution of the produced HP aqueous [1-13C]pyruvate solution, representing one additional limitation of the study. However, the [1-13C]pyruvate hyperpolarization experiments in Figure 2 are on a scale 6× larger than that employed in the purification experiments in Figure 5—this level and quantity of hyperpolarization is already sufficient for pilot in vivo experiments. Indeed, tail-vein injections of ¹³C HP [1-¹³C]pyruvate using PHIP-SAH hyperpolarization technology employed 0.24 mL injection mouse dose with P_{13C} of 9.7 \pm 1.5% (at the time of hyperpolarization) and $3.5 \pm 0.5\%$ at the time of the injection and pyruvate concentration of 35 ± 5 mM.²⁴ This mouse dose was sufficient for acquiring ¹³C MRI maps of [1-¹³C]pyruvate and [1-13C]lactate in a mouse model of dilated cardiomyopathy.2

CONCLUSION

We have demonstrated that Re-Dissolution (Re-D, pronounced "ready") SABRE-SHEATH efficiently enables extracting HP [1-13C]pyruvate—a most promising biosensor for future diagnostics of cancer, cardiac, and neurodegenerative disease patients—into an aqueous phase with P_{13C} of up to 9%. This approach shines in its simplicity, since no hydrogenation reaction or any chemical modification of the substrate molecule is needed for this technique compared to PHIP-SAH. Moreover, the presented approach is substantially faster compared to the leading d-DNP technique. While the approach would likely benefit from further refinement of the protocol (e.g., further reduction of solvent/catalyst content and improvement of degree of polarization) for in vivo applications, we anticipate that future automation efforts (using already demonstrated approaches for different PHIP techniques⁴⁷) will provide a robust procedure to prepare biocompatible HP [1-13C]pyruvate biosensor formulations for use in next-generation molecular imaging modalities that are both affordable and accessible for clinical utilization.

ASSOCIATED CONTENT

Supporting Information

The Supporting Information is available free of charge at https://pubs.acs.org/doi/10.1021/acssensors.2c01715.

Additional experimental details, materials, and methods, including photographs of extracted solutions (PDF)

AUTHOR INFORMATION

Corresponding Authors

Andreas B. Schmidt – Integrative Biosciences (Ibio), Department of Chemistry, Karmanos Cancer Institute (KCI), Wayne State University, Detroit, Michigan 48202, United States; German Cancer Consortium (DKTK), Partner Site Freiburg, German Cancer Research Center (DKFZ), Heidelberg 69120, Germany; Division of Medical Physics, Department of Radiology, Medical Center, University of Freiburg, Faculty of Medicine, University of Freiburg, Freiburg 79106, Germany; orcid.org/0000-0001-8944-7463; Email: andreas.schmidt@uniklinik-freiburg.de

Eduard Y. Chekmenev — Integrative Biosciences (Ibio),
Department of Chemistry, Karmanos Cancer Institute (KCI),
Wayne State University, Detroit, Michigan 48202, United
States; Russian Academy of Sciences (RAS), 119991 Moscow,
Russia; orcid.org/0000-0002-8745-8801;
Email: chekmenevlab@gmail.com

Authors

Henri de Maissin — German Cancer Consortium (DKTK), Partner Site Freiburg, German Cancer Research Center (DKFZ), Heidelberg 69120, Germany; Division of Medical Physics, Department of Radiology, Medical Center, University of Freiburg, Faculty of Medicine, University of Freiburg, Freiburg 79106, Germany

Isaiah Adelabu — Integrative Biosciences (Ibio), Department of Chemistry, Karmanos Cancer Institute (KCI), Wayne State University, Detroit, Michigan 48202, United States

Shiraz Nantogma – Integrative Biosciences (Ibio), Department of Chemistry, Karmanos Cancer Institute (KCI), Wayne State University, Detroit, Michigan 48202, United States

Jessica Ettedgui – Chemistry and Synthesis Center, National Heart, Lung, Blood Institute, Rockville, Maryland 20850, United States

Patrick TomHon – Department of Chemistry, North Carolina State University, Raleigh, North Carolina 27606, United States; Vizma Life Sciences LLC, Durham, North Carolina 27707-3669, United States; orcid.org/0000-0003-3202-9812

Boyd M. Goodson — School of Chemical & Biomolecular Sciences and Materials Technology Center, Southern Illinois University, Carbondale, Illinois 62901, United States; orcid.org/0000-0001-6079-5077

Thomas Theis — Department of Chemistry, North Carolina State University, Raleigh, North Carolina 27606, United States; Joint Department of Biomedical Engineering, University of North Carolina at Chapel Hill and North Carolina State University, Raleigh, North Carolina 27695, United States; Occid.org/0000-0001-6779-9978

Complete contact information is available at: https://pubs.acs.org/10.1021/acssensors.2c01715

Author Contributions

*Investigation: ABS, HdM, IA, SN, JE. Data curation: ABS, EYC. Funding acquisition: ABS, BMG, TT, EYC. Conceptualization: ABS, EYC. Methodology: ABS, HdM, EYC. Resources: EYC. Supervision: BG, TT, EYC. Visualization: all authors. Discussion of results: all authors. Writing original draft: ABS, EYC. Review and editing: all authors. All authors have given approval to the final version of the manuscript. ABS and HdM contributed equally.

Notes

The authors declare the following competing financial interest(s): TT holds stock in Vizma Life Sciences LLC (VLS) and is President of VLS. PT holds stock in VLS and is VLS employee. EYC and BMG disclose stakes of ownership in XeUS Technologies, LTD.

ACKNOWLEDGMENTS

This work received funding/financial support from the German Cancer Consortium (DKTK), B.E.S.T. Fluidsysteme GmbH I Swagelok Stuttgart, and the German Research Foundation (DFG grant numbers: SCHM 3694/1-1, SCHM 3694/2-1, SFB1479), NSF CHE-1904780 and CHE-1905341, NIH S10OD028488, and NIBIB R01EB029829. The content is solely the responsibility of the authors and does not necessarily represent the official views of the NIH. ABS and EYC thank Wayne State University for Postdoctoral Fellow award. SN and EYC thank Wayne State University Thomas C. Rumble University Graduate Fellowship.

ABBREVIATIONS

d-DNP, dissolution Dynamic Nuclear Polarization; EtAc, ethyl acetate; HP, hyperpolarized; MFC, mass-flow controller; MR, magnetic resonance; PHIP, Parahydrogen Induced Polarization; SABRE, Signal Amplification By Reversible Exchange; SABRE-SHEATH, SABRE in SHield Enables Alignment Transfer to Heteronuclei; Re-D SABRE, redissolution SABRE; SAH, side arm hydrogenation

REFERENCES

- (1) Ardenkjær-Larsen, J. H.; Fridlund, B.; Gram, A.; Hansson, G.; Hansson, L.; Lerche, M. H.; Servin, R.; Thaning, M.; Golman, K. Increase in Signal-to-Noise Ratio of > 10,000 Times in Liquid-State NMR. *Proc. Natl. Acad. Sci. U.S.A.* **2003**, *100* (18), 10158–10163.
- (2) Shchepin, R. V.; Coffey, A. M.; Waddell, K. W.; Chekmenev, E. Y. Parahydrogen Induced Polarization of 1^{-13} C-Phospholactate-D2 for Biomedical Imaging with > 30,000,000-Fold NMR Signal Enhancement in Water. *Anal. Chem.* **2014**, *86* (12), 5601–5605.
- (3) Müller, C. A.; Hundshammer, C.; Braeuer, M.; Skinner, J. G.; Berner, S.; Leupold, J.; Düwel, S.; Nekolla, S. G.; Månsson, S.; Hansen, A. E.; von Elverfeldt, D.; Ardenkjaer-Larsen, J. H.; Schilling, F.; Schwaiger, M.; Hennig, J.; Hövener, J.-B. Dynamic 2D and 3D Mapping of Hyperpolarized Pyruvate to Lactate Conversion in Vivo with Efficient Multi-Echo Balanced Steady-State Free Precession at 3 T. NMR in Biomedicine 2020, 33 (6), No. e4291.
- (4) Skinner, J. G.; Menichetti, L.; Flori, A.; Dost, A.; Schmidt, A. B.; Plaumann, M.; Gallagher, F. A.; Hövener, J.-B. Metabolic and Molecular Imaging with Hyperpolarised Tracers. *Mol. Imaging Biol.* **2018**, 20 (6), 902–918.
- (5) Nikolaou, P.; Goodson, B. M.; Chekmenev, E. Y. NMR Hyperpolarization Techniques for Biomedicine. *Chem.—Eur. J.* **2015**, 21 (8), 3156–3166.
- (6) Golman, K.; in 't Zandt, R.; Thaning, M. Real-Time Metabolic Imaging. *Proc. Natl. Acad. Sci. U.S.A.* **2006**, *103* (30), 11270–11275.
- (7) Hune, T.; Mamone, S.; Schroeder, H.; Jagtap, A. P.; Sternkopf, S.; Stevanato, G.; Korchak, S.; Fokken, C.; Müller, C. A.; Schmidt, A. B.; Becker, D.; Glöggler, S. Metabolic Tumor Imaging with Rapidly Signal-Enhanced 1–13C-Pyruvate-D3. *ChemPhysChem* **2022**, 615 DOI: 10.1002/cphc.202200615.
- (8) Day, S. E.; Kettunen, M. I.; Gallagher, F. A.; Hu, D.-E.; Lerche, M.; Wolber, J.; Golman, K.; Ardenkjaer-Larsen, J. H.; Brindle, K. M. Detecting Tumor Response to Treatment Using Hyperpolarized ¹³C Magnetic Resonance Imaging and Spectroscopy. *Nature Medicine* **2007**, *13* (11), 1382–1387.
- (9) Albers, M. J.; Bok, R.; Chen, A. P.; Cunningham, C. H.; Zierhut, M. L.; Zhang, V. Y.; Kohler, S. J.; Tropp, J.; Hurd, R. E.; Yen, Y.-F.; Nelson, S. J.; Vigneron, D. B.; Kurhanewicz, J. Hyperpolarized ¹³C Lactate, Pyruvate, and Alanine: Noninvasive Biomarkers for Prostate Cancer Detection and Grading. *Cancer Res.* **2008**, *68* (20), 8607–8615.
- (10) Kurhanewicz, J.; Vigneron, D. B.; Ardenkjaer-Larsen, J. H.; Bankson, J. A.; Brindle, K.; Cunningham, C. H.; Gallagher, F. A.; Keshari, K. R.; Kjaer, A.; Laustsen, C.; Mankoff, D. A.; Merritt, M. E.;

- Nelson, S. J.; Pauly, J. M.; Lee, P.; Ronen, S.; Tyler, D. J.; Rajan, S. S.; Spielman, D. M.; Wald, L.; Zhang, X.; Malloy, C. R.; Rizi, R. Hyperpolarized ¹³C MRI: Path to Clinical Translation in Oncology. *Neoplasia* **2019**, *21* (1), 1–16.
- (11) Jannin, S.; Bornet, A.; Melzi, R.; Bodenhausen, G. High Field Dynamic Nuclear Polarization at 6.7T: Carbon-13 Polarization above 70% within 20min. *Chem. Phys. Lett.* **2012**, *549*, 99–102.
- (12) Cheng, T.; Gaunt, A. P.; Marco-Rius, I.; Gehrung, M.; Chen, A. P.; van der Klink, J. J.; Comment, A. Multi-Sample 7 T DNP Polarizer for Preclinical Hyperpolarized MR. *NMR Biomed* **2020**, 33 (5), No. e4264
- (13) Ardenkjær-Larsen, J. H.; Bowen, S.; Petersen, J. R.; Rybalko, O.; Vinding, M. S.; Ullisch, M.; Nielsen, N. Chr. Cryogen-free Dissolution Dynamic Nuclear Polarization Polarizer Operating at 3.35 T, 6.70 T, and 10.1 T. *Magn. Reson. Med.* 2019, 81 (3), 2184–2194. (14) Hale, W. G.; Zhao, T. Y.; Choi, D.; Ferrer, M.-J.; Song, B.; Zhao, H.; Hagelin-Weaver, H. E.; Bowers, C. R. Toward Continuous-Flow Hyperpolarisation of Metabolites via Heterogenous Catalysis, Side-Arm-Hydrogenation, and Membrane Dissolution of Para-
- hydrogen. *ChemPhysChem* **2021**, 22 (9), 822–827. (15) Schmidt, A. B.; Zimmermann, M.; Berner, S.; de Maissin, H.; Müller, C. A.; Ivantaev, V.; Hennig, J.; Elverfeldt, D. v; Hövener, J.-B. Quasi-Continuous Production of Highly Hyperpolarized Carbon-13 Contrast Agents Every 15 Seconds within an MRI System. *Commun. Chem.* **2022**, 5 (1), 1–7.
- (16) Schmidt, A. B.; Bowers, C. R.; Buckenmaier, K.; Chekmenev, E. Y.; de Maissin, H.; Eills, J.; Ellermann, F.; Glöggler, S.; Gordon, J. W.; Knecht, S.; Koptyug, I. V.; Kuhn, J.; Pravdivtsev, A. N.; Reineri, F.; Theis, T.; Them, K.; Hövener, J.-B. Instrumentation for Hydrogenative Parahydrogen-Based Hyperpolarization Techniques. *Anal. Chem.* **2022**, *94* (1), 479–502.
- (17) Bowers, C. R.; Weitekamp, D. P. Parahydrogen and Synthesis Allow Dramatically Enhanced Nuclear Alignment. *J. Am. Chem. Soc.* 1987, 109 (18), 5541–5542.
- (18) Eisenschmid, T. C.; Kirss, R. U.; Deutsch, P. P.; Hommeltoft, S. I.; Eisenberg, R.; Bargon, J.; Lawler, R. G.; Balch, A. L. Para Hydrogen Induced Polarization in Hydrogenation Reactions. *J. Am. Chem. Soc.* 1987, 109 (26), 8089–8091.
- (19) Reineri, F.; Boi, T.; Aime, S. ParaHydrogen Induced Polarization of ¹³C Carboxylate Resonance in Acetate and Pyruvate. *Nat. Commun.* **2015**, *6*, 5858.
- (20) Korchak, S.; Mamone, S.; Glöggler, S. Over 50% ¹H and ¹³C Polarization for Generating Hyperpolarized Metabolites—A Para-Hydrogen Approach. *ChemistryOpen* **2018**, 7 (9), 672–676.
- (21) Joalland, B.; Schmidt, A. B.; Kabir, M. S. H.; Chukanov, N. V.; Kovtunov, K. V.; Koptyug, I. V.; Hennig, J.; Hövener, J.-B.; Chekmenev, E. Y. Pulse-Programmable Magnetic Field Sweeping of Parahydrogen-Induced Polarization by Side Arm Hydrogenation. *Anal. Chem.* **2020**, 92 (1), 1340–1345.
- (22) Schmidt, A. B.; Brahms, A.; Ellermann, F.; Knecht, S.; Berner, S.; Hennig, J.; von Elverfeldt, D.; Herges, R.; Hovener, J.-B.; Pravdivtsev, A. N. Selective Excitation of Hydrogen Doubles the Yield and Improves the Robustness of Parahydrogen-Induced Polarization of Low-γ Nuclei. *Phys. Chem. Chem. Phys.* **2021**, 23, 26645.
- (23) Carrera, C.; Cavallari, E.; Digilio, G.; Bondar, O.; Aime, S.; Reineri, F. ParaHydrogen Polarized Ethyl-[1–¹³C]Pyruvate in Water, a Key Substrate for Fostering the PHIP-SAH Approach to Metabolic Imaging. *ChemPhysChem* **2021**, 22 (11), 1042–1048.
- (24) Cavallari, E.; Carrera, C.; Sorge, M.; Bonne, G.; Muchir, A.; Aime, S.; Reineri, F. The ¹³C Hyperpolarized Pyruvate Generated by ParaHydrogen Detects the Response of the Heart to Altered Metabolism in Real Time. *Sci. Rep.* **2018**, 8 (1), 8366.
- (25) Dagys, L.; Jagtap, A. P.; Korchak, S.; Mamone, S.; Saul, P.; Levitt, M. H.; Glöggler, S. Nuclear Hyperpolarization of $(1^{-13}C)$ -Pyruvate in Aqueous Solution by Proton-Relayed Side-Arm Hydrogenation. *Analyst* **2021**, *146* (5), 1772–1778.
- (26) Ding, Y.; Korchak, S.; Mamone, S.; Jagtap, A. P.; Stevanato, G.; Sternkopf, S.; Moll, D.; Schroeder, H.; Becker, S.; Fischer, A.;

ı

- Gerhardt, E.; Outeiro, T. F.; Opazo, F.; Griesinger, C.; Glöggler, S. Rapidly Signal-Enhanced Metabolites for Atomic Scale Monitoring of Living Cells with Magnetic Resonance. *Chemistry-Methods* **2022**, *2*, No. e202200023.
- (27) Cavallari, E.; Carrera, C.; Aime, S.; Reineri, F. Metabolic Studies of Tumor Cells Using [1–¹³C] Pyruvate Hyperpolarized by Means of PHIP-Side Arm Hydrogenation. *ChemPhysChem* **2019**, 20 (2), 318–325.
- (28) Mamone, S.; Jagtap, A. P.; Korchak, S.; Ding, Y.; Sternkopf, S.; Glöggler, S. A Field-Independent Method for the Rapid Generation of Hyperpolarized $[1-^{13}C]$ Pyruvate in Clean Water Solutions for Biomedical Applications. *Angew. Chem.* **2022**, *134*, 6298 DOI: 10.1002/ange.202206298.
- (29) Adams, R. W.; Aguilar, J. A.; Atkinson, K. D.; Cowley, M. J.; Elliott, P. I. P.; Duckett, S. B.; Green, G. G. R.; Khazal, I. G.; López-Serrano, J.; Williamson, D. C. Reversible Interactions with Para-Hydrogen Enhance NMR Sensitivity by Polarization Transfer. *Science* **2009**, 323 (5922), 1708–1711.
- (30) Theis, T.; Truong, M. L.; Coffey, A. M.; Shchepin, R. V.; Waddell, K. W.; Shi, F.; Goodson, B. M.; Warren, W. S.; Chekmenev, E. Y. Microtesla SABRE Enables 10% Nitrogen-15 Nuclear Spin Polarization. J. Am. Chem. Soc. 2015, 137 (4), 1404–1407.
- (31) Adelabu, I.; TomHon, P.; Kabir, M. S. H.; Nantogma, S.; Abdulmojeed, M.; Mandzhieva, I.; Ettedgui, J.; Swenson, R. E.; Krishna, M. C.; Theis, T.; Goodson, B. M.; Chekmenev, E. Y. Order-Unity ¹³C Nuclear Polarization of [1–¹³C]Pyruvate in Seconds and the Interplay of Water and SABRE Enhancement. *ChemPhysChem* **2022**, 23 (2), No. e202100839.
- (32) Iali, W.; Roy, S. S.; Tickner, B. J.; Ahwal, F.; Kennerley, A. J.; Duckett, S. B. Hyperpolarising Pyruvate through Signal Amplification by Reversible Exchange (SABRE). *Angew. Chem.* **2019**, *131* (30), 10377–10381.
- (33) Chapman, B.; Joalland, B.; Meersman, C.; Ettedgui, J.; Swenson, R. E.; Krishna, M. C.; Nikolaou, P.; Kovtunov, K. V.; Salnikov, O. G.; Koptyug, I. V.; Gemeinhardt, M. E.; Goodson, B. M.; Shchepin, R. V.; Chekmenev, E. Y. Low-Cost High-Pressure Clinical-Scale 50% Parahydrogen Generator Using Liquid Nitrogen at 77 K. *Anal. Chem.* 2021, 93 (24), 8476–8483.
- (34) TomHon, P.; Abdulmojeed, M.; Adelabu, I.; Nantogma, S.; Kabir, M. S. H.; Lehmkuhl, S.; Chekmenev, E. Y.; Theis, T. Temperature Cycling Enables Efficient ¹³C SABRE-SHEATH Hyperpolarization and Imaging of [1–¹³C]-Pyruvate. *J. Am. Chem. Soc.* **2022**, *144* (1), 282–287.
- (35) Barskiy, D. A.; Ke, L. A.; Li, X.; Stevenson, V.; Widarman, N.; Zhang, H.; Truxal, A.; Pines, A. Rapid Catalyst Capture Enables Metal-Free Para-Hydrogen-Based Hyperpolarized Contrast Agents. *J. Phys. Chem. Lett.* **2018**, 9 (11), 2721–2724.
- (36) Kidd, B. E.; Gesiorski, J. L.; Gemeinhardt, M. E.; Shchepin, R. V.; Kovtunov, K. V.; Koptyug, I. V.; Chekmenev, E. Y.; Goodson, B. M. Facile Removal of Homogeneous SABRE Catalysts for Purifying Hyperpolarized Metronidazole, a Potential Hypoxia Sensor. *J. Phys. Chem. C* 2018, 122 (29), 16848–16852.
- (37) Manoharan, A.; Rayner, P. J.; Iali, W.; Burns, M. J.; Perry, V. H.; Duckett, S. B. Achieving Biocompatible SABRE: An in Vitro Cytotoxicity Study. *ChemMedChem.* **2018**, *13* (4), 352–359.
- (38) Nantogma, S.; Joalland, B.; Wilkens, K.; Chekmenev, E. Y. Clinical-Scale Production of Nearly Pure (>98.5%) Parahydrogen and Quantification by Benchtop NMR Spectroscopy. *Anal. Chem.* **2021**, 93 (7), 3594–3601.
- (39) Hövener, J.-B.; Schwaderlapp, N.; Borowiak, R.; Lickert, T.; Duckett, S. B.; Mewis, R. E.; Adams, R. W.; Burns, M. J.; Highton, L. A. R.; Green, G. G. R.; Olaru, A.; Hennig, J.; von Elverfeldt, D. Toward Biocompatible Nuclear Hyperpolarization Using Signal Amplification by Reversible Exchange: Quantitative in Situ Spectroscopy and High-Field Imaging. *Anal. Chem.* 2014, 86 (3), 1767–1774. (40) Truong, M. L.; Shi, F.; He, P.; Yuan, B.; Plunkett, K. N.; Coffey, A. M.; Shchepin, R. V.; Barskiy, D. A.; Kovtunov, K. V.; Koptyug, I. V.; Waddell, K. W.; Goodson, B. M.; Chekmenev, E. Y. Irreversible

Catalyst Activation Enables Hyperpolarization and Water Solubility

- for NMR Signal Amplification by Reversible Exchange. J. Phys. Chem. B 2014, 118 (48), 13882–13889.
- (41) Colell, J. F. P.; Emondts, M.; Logan, A. W. J.; Shen, K.; Bae, J.; Shchepin, R. V.; Ortiz, G. X.; Spannring, P.; Wang, Q.; Malcolmson, S. J.; Chekmenev, E. Y.; Feiters, M. C.; Rutjes, F. P. J. T.; Blümich, B.; Theis, T.; Warren, W. S. Direct Hyperpolarization of Nitrogen-15 in Aqueous Media with Parahydrogen in Reversible Exchange. *J. Am. Chem. Soc.* **2017**, *139* (23), 7761–7767.
- (42) Zeng, H.; Xu, J.; McMahon, M. T.; Lohman, J. A. B.; van Zijl, P. C. M. Achieving 1% NMR Polarization in Water in Less than 1min Using SABRE. J. Magn. Reson. 2014, 246, 119–121.
- (43) Spannring, P.; Reile, I.; Emondts, M.; Schleker, P. P. M.; Hermkens, N. K. J.; van der Zwaluw, N. G. J.; van Weerdenburg, B. J. A.; Tinnemans, P.; Tessari, M.; Blümich, B.; Rutjes, F. P. J. T.; Feiters, M. C. A New Ir-NHC Catalyst for Signal Amplification by Reversible Exchange in D₂O. *Chem.—Eur. J.* 2016, 22 (27), 9277–9282.
- (44) Lin, K.; TomHon, P.; Lehmkuhl, S.; Laasner, R.; Theis, T.; Blum, V. Density Functional Theory Study of Reaction Equilibria in Signal Amplification by Reversible Exchange. *ChemPhysChem* **2021**, 22 (19), 1947–1957.
- (45) Shi, F.; He, P.; Best, Q. A.; Groome, K.; Truong, M. L.; Coffey, A. M.; Zimay, G.; Shchepin, R. V.; Waddell, K. W.; Chekmenev, E. Y.; Goodson, B. M. Aqueous NMR Signal Enhancement by Reversible Exchange in a Single Step Using Water-Soluble Catalysts. *J. Phys. Chem. C* 2016, 120 (22), 12149–12156.
- (46) Eills, J.; Alonso-Valdesueiro, J.; Salazar Marcano, D. E.; Ferreira da Silva, J.; Alom, S.; Rees, G. J.; Hanna, J. V.; Carravetta, M.; Levitt, M. H. Preservation of Nuclear Spin Order by Precipitation. *ChemPhysChem* **2018**, *19* (1), 40–44.
- (47) Knecht, S.; Blanchard, J. W.; Barskiy, D.; Cavallari, E.; Dagys, L.; Van Dyke, E.; Tsukanov, M.; Bliemel, B.; Munnemann, K.; Aime, S.; Reineri, F.; Levitt, M. H.; Buntkowsky, G.; Pines, A.; Blumler, P.; Budker, D.; Eills, J. Rapid Hyperpolarization and Purification of the Metabolite Fumarate in Aqueous Solution. *Proc. Natl. Acad. Sci. U.S.A.* **2021**, *118* (13), 1 DOI: 10.1073/pnas.2025383118.
- (48) Bondar, O.; Cavallari, E.; Carrera, C.; Aime, S.; Reineri, F. Effect of the Hydrogenation Solvent in the PHIP-SAH Hyper-polarization of $[1-^{13}C]$ Pyruvate. Catal. Today 2022, 397-399, 94.